Journal of Pathology
J Pathol 2020; **251**: 440–451
Published online 30 June 2020 in Wiley Online Library (wileyonlinelibrary.com) DOI: 10.1002/path.5478

ORIGINAL PAPER

Histological 3D reconstruction and *in vivo* lineage tracing of the human endometrium

Nicola Tempest[1,2], Marnix Jansen[3], Ann-Marie Baker[4], Christopher J. Hill[2], Mike Hale[5], Derek Magee[6,7], Darren Treanor[5,8,9], Nicholas A. Wright[4] and Dharani K. Hapangama[1,2*]

[1] *Liverpool Women's Hospital NHS Foundation Trust, member of the Liverpool Health partnership, Liverpool, UK*
[2] *Department of Women's and Children's Health, Institute of Life Course and Medical Sciences, University of Liverpool, member of the Liverpool Health partnership, Liverpool, UK*
[3] *UCL Cancer Institute, University College London, London, UK*
[4] *Barts Cancer Institute, Barts and the London School of Medicine and Dentistry, Queen Mary University of London, London, UK*
[5] *Pathology and Tumour Biology, University of Leeds, Leeds, UK*
[6] *School of Computing, University of Leeds, Leeds, UK*
[7] *Heterogenius Ltd, Leeds, UK*
[8] *Pathology department, Leeds Teaching Hospitals NHS Trust, Leeds, UK*
[9] *Pathology department, Linköping University, Linköping, Sweden*

**Correspondence to: DK Hapangama, Department of Women's and Children's Health, Institute of Translational Medicine, University of Liverpool, Liverpool L8 7SS, UK. E-mail: dharani@liv.ac.uk*

Abstract

Regular menstrual shedding and repair of the endometrial functionalis is unique to humans and higher-order primates. The current consensus postulates endometrial glands to have a single-tubular architecture, where multi-potential stem cells reside in the blind-ending glandular-bases. Utilising fixed samples from patients, we have studied the three-dimensional (3D) micro-architecture of the human endometrium. We demonstrate that some non-branching, single, vertical functionalis glands originate from a complex horizontally interconnecting network of basalis glands. The existence of a multipotent endometrial epithelial stem cell capable of regenerating the entire complement of glandular lineages was demonstrated by *in vivo* lineage tracing, using naturally occurring somatic mitochondrial DNA mutations as clonal markers. Vertical tracking of mutated clones showed that at least one stem-cell population resides in the basalis glands. These novel findings provide insight into the efficient and scar-less regenerative potential of the human endometrium.

Keywords: 3D reconstruction; lineage tracing; endometrium; regeneration; stem cells

Received 19 December 2019; Revised 30 April 2020; Accepted 20 May 2020

No conflicts of interest were declared.

Introduction

The endometrium is a highly regenerative tissue that undergoes more than 400 monthly cycles of proliferation and sloughing under the influence of ovarian hormones during a woman's lifetime. The current consensus envisages that human endometrial stem cells are responsible for this efficient regeneration. Epithelial stem cells are postulated to reside in the terminal ends of the blind-ended single-tubular endometrial glands at the endometrial/myometrial interface [1–4], analogous to the structural organisation of intestinal crypts. However, the precise three-dimensional (3D) anatomical micro-architectural organisation of the human endometrial glandular mucosa is unknown. Attempts have been made previously to investigate human endometrial epithelial cell lineages utilising two methods. Tanaka *et al* explored the clonality of epithelial cells by analysing DNA extracted from individual endometrial glands using the X-linked androgen receptor gene as an indirect marker of non-random X chromosome inactivation, and reported on the clonal constitution of glandular cells and luminal epithelium (LE) [5]; Kim *et al* proposed that cell divisions and ancestry may be surreptitiously recorded by identifying replication errors that naturally accumulate in a clock-like manner during aging based on the hypothesis that all daughter cells originate from a common ancestor [3,5]. These studies implicitly assume the endometrial glandular organisation to be blind-ending single tubes, a hypothesis yet to be confirmed. Understanding the 3D structure of the endometrium has contributed to our current perception of embryo implantation and postnatal glandular morphogenesis in mice [6,7]. Notably, confocal imaging and consequent 3D renderings of optical sections of

endometrial glands revealed increased glandular complexity of the human uterus compared with mouse [6].

Menstrual shedding and subsequent repair of the endometrial functionalis layer is a process unique to humans and higher-order primates. This distinctive regeneration pattern makes traditional *in vivo* lineage tracing studies in rodent models, that confirm the existence of an adult epithelial stem cell, less relevant to the human endometrium [8–12]. An *in vivo* lineage tracing method applicable to human solid organs has been developed, which overcomes this barrier, where the progeny of a stem cell is directly identified in intact tissue by tracing mitochondrial DNA (mtDNA) mutations in the epithelial compartment. Spontaneously arising mutations in the mitochondrially encoded cytochrome *c* oxidase (*CCO*) gene—an enzyme forming the last step of the electron transport chain in respiratory complex IV—could be used to directly visualize cell lineages in renewing stem cell systems [13]. This assay requires mutation of 80% of *CCO* genes for a cell to be identified as deficient, a process that takes decades to develop; thus the ancestral cell giving rise to a CCO-deficient clonal patch has to be long-lived [13]. By definition, in a dynamic tissue that has a high cell turn-over, stem cells are the oldest cells. This method allows lineages to be traced and, in several instances previously, the stem cell niche to be identified [13–18].

Because aberrations in stem cells that regularly regenerate the functionalis layer are postulated to play a role in most endometrial pathologies [4], expansion of our current understanding of stem cells is necessary for curative treatment strategies to be developed. We aimed to address deficiencies in current human endometrial stem cell literature; initially we performed 3D tissue reconstruction, utilising fixed histological samples of the human adult endometrium to reveal the architectural organisation of the entire glandular element in premenopausal endometrium with all functional components as well as the postmenopausal (PM) endometrium containing the stem cell rich basalis. Our data revealed a previously unknown complex, branching, intricate and interwoven 3D configuration of the basalis glands that runs a horizontal course along the myometrium, compelling the current consensus to be incorrect. We then performed *in vivo* lineage tracing using mtDNA mutations as clonal markers, exploiting spontaneously occurring *CCO* gene mutations that are inherited by daughter cells [13,15,17] allowing us to identify the adult stem cell niche in the endometrial epithelium. Finally we examined the differentiation potential of the stem cell progeny and involvement of dedicated stem cells in the regeneration of the entire human endometrial glandular element and the natural history of clonal patch dynamics.

Materials and methods

Tissue samples

Full-thickness human endometrial samples were collected from 104 women undergoing benign gynecological surgery with no endometrial pathology who did not use hormonal medications for 3 months prior to hysterectomy at the Liverpool Women's Hospital with collection approved by Liverpool Adult Ethics committee (REC references; 09/H1005/55 and 11/H1005/4) (see supplementary material, Table S1). The cycle phase of the endometrium was assigned according to the last menstrual period (LMP) and histological criteria [19,20].

Immunohistochemistry

Standard hematoxylin and eosin (H&E) histology and immunohistochemistry were performed as previously described [1,13] (for antibody information see supplementary material, Table S2). For chromogenic staining, antigen retrieval was performed on sections of formalin-fixed paraffin-embedded (FFPE) tissues, cut at 4 μm. Dried sections were dewaxed, rehydrated, and then blocked with 3% hydrogen peroxide (Thermo Fisher Scientific, Runcorn, UK) for 10 min, prior to incubation with diluted primary antibody as indicated in supplementary material, Table S2. After rinsing, the appropriate secondary antibody was applied for 30 min at room temperature (RT). Detection used the ImmPRESS polymer-based system, and visualisation was with ImmPACT DAB, following the manufacturer's instructions (Vector Laboratories, Peterborough, UK). Sections were counterstained using Gill II Hematoxylin (Thermo Fisher Scientific), and then dehydrated, cleared, and mounted in Consul-Mount (Thermo Fisher Scientific). Matching isotype replaced primary antibody as a negative control, with internal positive control in each staining run.

The Ki-67 labeling index was evaluated as the percentage of immunopositive cells, of any intensity. The entire section was evaluated at 400× magnification as described previously [21].

Immunofluorescence staining was performed on 4 μm sequential sections of FFPE tissues. After antigen retrieval, sections were blocked and stained with the appropriate primary antibodies (see supplementary material, Table S2). Mouse and rabbit IgGs (Vector Laboratories) served as isotype controls. The secondary antibodies were Alexa Fluor 488 and 555 anti-rabbit and anti-mouse (Cell Signaling Technology, London, UK) at 1:1000 dilution. Secondary antibodies were incubated for 2 h at room temperature and sections were mounted in Vectashield with DAPI (Vector Laboratories). Imaging was performed on a Nikon Eclipse 50i microscope.

In situ hybridisation (ISH)

ISH to detect the mRNA for leucine-rich repeat-containing G protein–coupled receptor 5 (*LGR5)*, which is a marker of stem cells in various epithelia [22] was performed as, described previously [23] on 4 μm sections using RNAscope 2.5 High Definition Brown assays, according to the manufacturer's instructions (Advanced Cell Diagnostics, Hayward, CA). Samples were baked at 60 °C for 90 min, followed by dewaxing and incubation with Pretreat 1 buffer for 10 min at RT. Slides were

boiled in Pretreat 2 buffer for 15 min, followed by incubation with Pretreat 3 buffer, for 15 min at 40 °C. Slides were incubated with the relevant probes for 2 h at 40 °C, followed by successive incubations with Amp 1–6 reagents. The colour reaction used 3, 3'-diaminobenzidine (DAB) for 20 min, and sections were counterstained lightly with Gill I Haemotoxylin (Thermo Fisher Scientific). The RNAscope probes used were *LGR5* (NM_003667.2, region 560-1589 catalogue number 311021), *POLR2A* (positive control probe) (NM_000937.4, region 2514-3433 catalogue number 310451), and *dapB* (negative control probe) (EF191515, region 414-862, catalogue number 310043).

LGR5 expression was quantified according to the 5-grade scoring system recommended by the manufacturer: (0 = No staining or less than 1 dot to every 10 cells (40× magnification), 1 = 1–3 dots/cell (visible at 20–40× magnification), 2 = 4–10 dots/cell, very few dot clusters (visible at 20–40× magnification), 3 = >10 dots/cell, less than 10% positive cells have dot clusters (visible at 20× magnification), 4 = >10 dots/cell, more than 10% positive cells have dot clusters (visible at 20× magnification)), as described previously [23].

3D modelling

One hundred consecutive sections were scanned using an Aperio ScanScope slide scanner (Aperio Technologies, Vista, CA, USA) at 400× magnification, creating virtual slides. The virtual slides were sent to the Leeds Institute of Cancer and Pathology, where they underwent the process of registration, and aligning in stacks, so that two-dimensional (2D) features were aligned to form smooth 3D topographies. This registration resulted in a stack of images that had been aligned, and thus could be rendered in 3D as a 3D 'volume'. The virtual slides were registered using Medical Image Manager (www.heterogenius.co.uk/MIM). A reference image was selected in the middle of the image stack and used to align subsequent images proceeding out from the centre, aligning all images to their neighbours. This aligned each virtual slide to adjacent slides within the data set, before the images were uploaded into Free-D16 240 software program [24] for 3D reconstruction. The method was as follows: serial images (TIFF file format) were imported into Free-D software v 1.10 image stack files. Endometrial gland boundaries, in a specific area on the individual sections of full-thickness endometrium, were drawn manually in each 2D serial image, and connected along the third dimension, between adjacent slides, producing 3D models.

The different anatomical areas of the full thickness endometrial samples were examined with specific reference to the two different epithelial compartments, the *functionalis* (typically in a secretory phase sample, glands in the upper 2/3 of the endometrium below the LE, surrounded by sparse stroma) and the *basalis* (glands in the lower 1/3 of the secretory phase endometrium adjacent to the endo-myometrial junction, surrounded by densely packed stroma and the location of this basalis-functionalis boundary displayed the well-known variation according to the menstrual cycle phase) in greater detail, relating to the architecture of the gland profiles, and their interactions.

Enzyme histochemistry

Enzyme histochemistry for CCO was performed as described previously [17] on 12-µm-thick sections of frozen full-thickness endometrium incubated, first in CCO medium (100 mM cytochrome *C*, 4 mM diaminobenzidine tetrahydrochloride, and 20 µg/ml catalase in 0.2 M phosphate buffer, pH 7.0 all from Sigma Aldrich, Poole, UK) at 37 °C for 50 min to allow for detection of CCO activity in brown, followed by washes in phosphate-buffered saline (PBS) pH7.4 (3 × 5 min). Second, sections were incubated in succinate dehydrogenase (SDH) medium (130 mM sodium succinate, 200 µM phenazine methosulphate, 1 mM sodium azide, 1.5 mM nitroblue tetrazolium in 0.2 M phosphate buffer, pH 7.0 all from Sigma Aldrich) at 37 °C for 40 min before further PBS washes (3× 5 min). Following this, sections were allowed to air-dry prior to laser capture microdissection (LCM), or dehydrated in a graded ethanol series (70%, 95%, 2 × 100%), cleared in Histoclear (Fisher Scientific, Leicestershire, UK), and mounted in DPX (BDH Laboratory Supplies, Poole, UK). This method, therefore, allowed CCO-proficient cells (wildtype) to be stained brown, and CCO-deficient areas to be highlighted, and recognised by detecting the activity of the nuclear-encoded enzyme, succinate dehydrogenase (SDH, blue, component of complex II of the respiratory chain).

Laser capture microdissection (LCM)

Single endometrial epithelial cells of interest (CCO proficient and deficient), and stroma for control, were cut and captured into sterile 0.5 ml AdhesiveCap PCR tubes (Carl Zeiss, Oberkochen, Germany) using a PALM Microbeam laser capture system (Carl Zeiss). Following LCM, 15 µl of ATL buffer (QIAamp DNA micro kit, Qiagen, Manchester, UK) was added to each sample, to commence cell lysis, and the samples were stored at −20 °C overnight, prior to DNA extraction using a Qiagen QIAamp DNA micro kit (Qiagen). The DNA in the collection tube was stored at −20 °C prior to PCR.

Sequencing of mtDNA from individual endometrial epithelia cells

The entire sequence of the mitochondrial genome from microdissected individual epithelial cells was determined using the single-cell lysate as the DNA template, and a two-stage amplification protocol.

The primary PCR reactions involved amplification of the mitochondrial genome in nine fragments of approximately 2 kbp, using a series of overlapping primer pairs. All PCR amplifications were performed in a 50 µl volume, containing 1× PCR buffer (10 mM Tris–HCl, pH 8.3, 1.5 mM $MgCl_2$, 50 mM KCl, 0.001% wt/vol gelatin),

0.2 mM dNTPs, 0.6 μM primers, 1 U AmpliTaq Gold DNA polymerase (all from Thermo Fisher Scientific), and 1 μl single-cell lysate. The secondary PCR reactions involved amplification of the primary PCR products with 28 primer pairs, specifically to generate overlapping fragments of between 600–700 base pairs that spanned the entire sequence of the human mitochondrial genome. To facilitate the direct sequencing of PCR-amplified products, all primer pairs were tagged with M13 sequence, and designed to anneal optimally at 58 °C.

Sequencing

Sanger sequencing used BigDye 3.1 terminator cycle-sequencing chemistries (Thermo Fisher Scientific) and an ABI 3730XL automated DNA sequencer, and was carried out by staff at Bart's Cancer Institute.

Sequences obtained were analysed using 4Peaks software (www.nucleobytes.com), together with Clustal W2 software (EMBL-EBI), and compared to the revised Cambridge reference sequence [25] with sequences from stromal controls and CCO-proficient specimens to identify polymorphisms and somatic mutations from the CCO-deficient sequences. Individual mutations were confirmed, in all instances, by repeating the first- and second-round PCRs, and resequencing the products.

Results

3D reconstruction of adult human endometrial glands

One hundred consecutive 4 μm sections from seven human endometrial samples (two proliferative, three secretory, and two PM) were stained and aligned prior to generating 3D models with Free-D16 240 software [24] as described previously [26,27]. All sections included full thickness of the human endometrial mucosa, from the lumen to the endometrial-myometrial junction incorporating the whole glandular element in the analysis. The region-specific orientation and branching pattern of the glands in these full-thickness endometrial samples are depicted in Table 1, and subsequent confirmatory 3D reconstruction (Figure 1) joining the 2D images along the third dimension allowed a more comprehensive delineation of the glands in order to draw conclusions. When traced from the sub-endometrial myometrium up to the endometrial functionalis/basalis junction, the deeper basalis glands demonstrated a complex, often branched organisation, enveloping one another horizontally in a mycelium/root–like configuration on the underlying myometrium (Figure 1A(i) and (ii) and see supplementary material, Video S1 and Figure 1A(iii) and (iv) and Video S2). The quiescent PM endometrium was also examined to scrutinise the current hypothesis that this is the remaining basalis. PM endometrium contained considerably fewer glands, but they seemed to show a similar branching pattern to the basalis pre-menopausal glands (see supplementary material, Figure S1 and Video S3). The more superficial, single lumen, vertical, functionalis glands were arranged at 90° angles to these basalis glands (Figure 1B(i) and (ii) and see supplementary material, Video S4 and Figure 1B (iii) and (iv) and see supplementary material, Video S5). The glands in the proliferative phase samples, (with high Ki67 proliferative indices, see supplementary material, Figure S2) were thinner, straighter, and easier to trace. In contrast, the non-proliferating functionalis glands of the secretory phase samples (with low Ki67 proliferative indices) [21,22] were longer, coiled, and showed wider lumens. These changes observed in secretory functionalis glands will have obvious functional significance because they are a source of nutrients, growth factors, and cytokines during embryo implantation and in the first trimester of human pregnancy [28]. This novel glandular arrangement thus replaces the existing, obsolescent schematic of the human endometrial glandular organisation.

Mitochondrial mutations confirm the existence of endometrial epithelial stem cells

The endometrial stem cell niche was determined by *in vivo* lineage tracing using non-pathogenic mtDNA mutations as clonal markers. This in effect, is a natural experiment, exploiting spontaneously occurring mutations in the *CCO* gene in long-lived stem cells, which are inherited by daughter cells to produce a CCO-deficient clonal patch, allowing the existence and the niche of stem cells to be identified. Partially mutated glands in

Table 1. The number, direction, and branching status of all the gland profiles identified and analysed across the 100 consecutive sections of the seven human endometrial full-thickness samples that were utilised in constructing 3D models.

Sample no.	Phase	Horizontal *funct.* gland profiles	Vertical *funct.* gland profiles	Branching *funct.* gland profiles	All *funct.* gland profiles	Horizontal *basalis* gland profiles	Vertical *basalis* gland profiles	Branching *basalis* gland profiles	All *basalis* gland profiles
1	Proliferative	31 (1.6%)	1963 (98.4%)	14 (0.7%)	1994 (100%)	4147 (95.9%)	178 (4.1%)	604 (14%)	4325 (100%)
2	Proliferative	54 (0.4%)	12 091 (99.6%)	46 (0.4%)	12 145 (100%)	3313 (98.7%)	44 (1.3%)	395 (11.8%)	3357 (100%)
3	Secretory	76 (0.6%)	13 682 (99.4%)	303 (2.2%)	13 758 (100%)	4941 (96.6%)	173 (3.4%)	854 (16.7%)	5114 (100%)
4	Secretory	93 (0.5%)	20 419 (99.5%)	100 (0.5%)	20 512 (100%)	8072 (97.3%)	228 (2.7%)	1040 (12.5%)	8300 (100%)
5	Secretory	185 (2.1%)	8792 (97.9%)	129 (1.4%)	8977 (100%)	5727 (96.3%)	223 (3.7%)	901 (15.1%)	5950 (100%)
6	PM	X	X	X	X	10 025 (94.2%)	621 (5.8%)	745 (7%)	10 646 (100%)
7	PM	X	X	X	X	3933 (95.8%)	173 (4.2%)	846 (20.6%)	4106 (100%)

PM, Post-menopausal; X, Not Applicable.

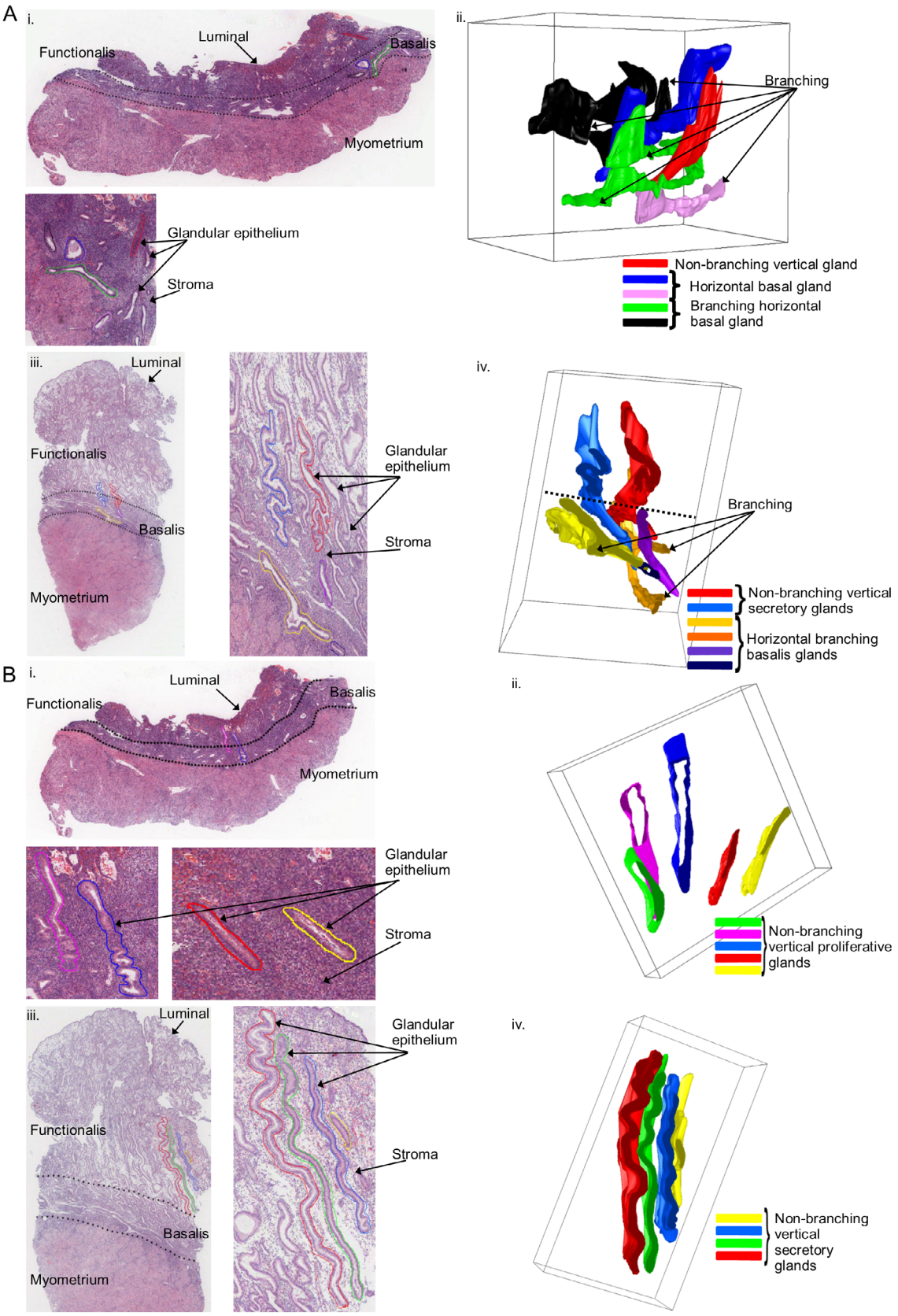

Figure 1. Micrographs and 3D model schematics depicting 3D architecture of premenopausal human endometrium. Human endometrial basalis glands form a complex and branching configuration, proceeding in a horizontal course to the myometrium enveloping one another, whereas the non-branching, single tubular functionalis glands rise vertically from the mycelium-like branching basalis glands, and run a parallel, vertical course through the superficial human endometrium. (A) basalis glands and (B) functionalis glands of the early-proliferative and secretory phase endometrium depicting low and high (i, iii) power micrographs and 3D schematics (ii, iv).

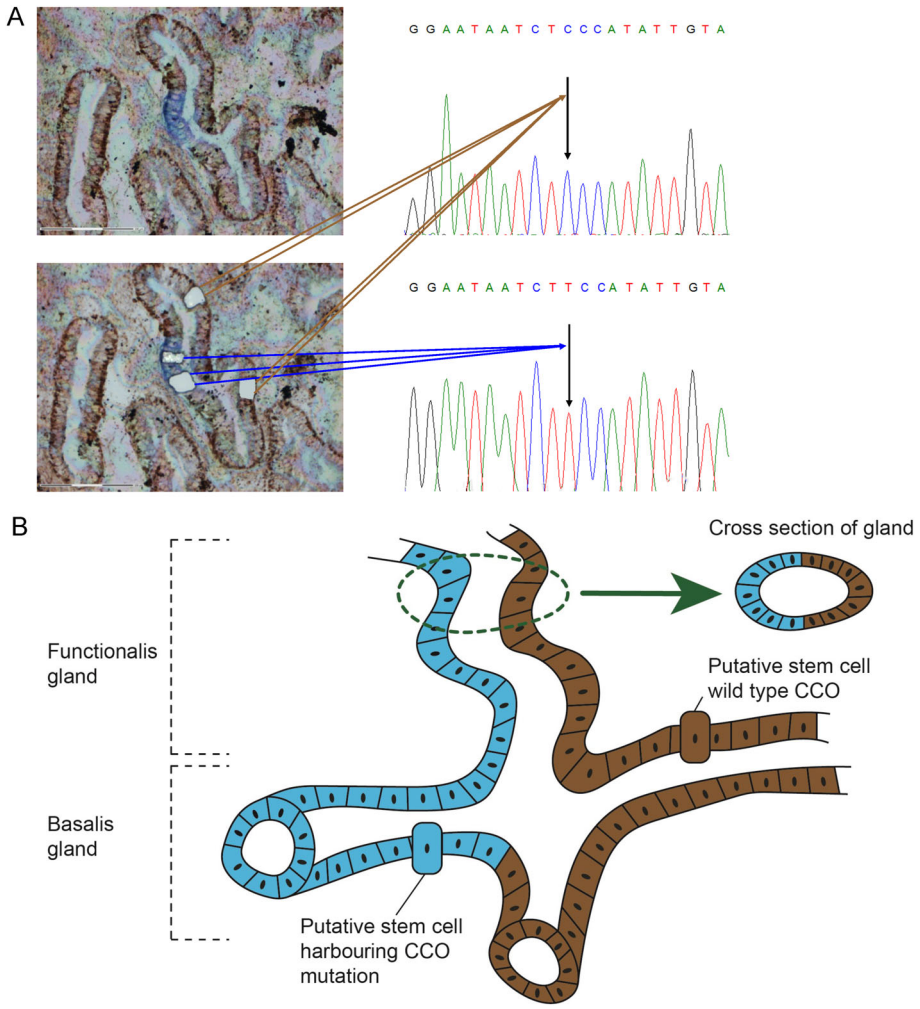

Figure 2. Confirmation of the existence of an epithelial stem cell with *in vivo* lineage tracing. (A) A unique mitochondrial mutation confirms the existence of endometrial epithelial stem cells in the endometrium. Representative images (left) and Sanger sequencing traces (right) showing wild-type brown-stained cytochrome-c-oxidase (CCO)-proficient cells with a `C` at position 6667 and blue-stained CCO-deficient cells with a `T` at position 6667, demonstrating a clonal expansion. (B) A schematic diagram demonstrating the speculated upward perpendicular growth of progeny of two stem cells situated in the parallel/ branching basalis glands giving rise to a partially mutated functionalis gland.

full-thickness frozen endometrial samples were utilised to demonstrate that collections of CCO-deficient cells represent *bona fide* clonal lineages (similar to the previous studies in other solid organs [13]). Multiple CCO-deficient (blue) cells were isolated using LCM alongside isolating multiple wild-type (brown) cells and stroma (as control tissue). Their entire mtDNA genome was sequenced to reveal common somatic mutations that indicate a common cell of origin. Figure 2A shows all of the microdissected cells (both neighbouring and distantly positioned cells) from the same CCO-deficient area of a partially mutated gland contain the same mtDNA mutation (c.6667C > T), which was not present in the surrounding CCO-proficient cells, demonstrating a clonal lineage within the CCO-deficient area. Previous work has established the calculated chance of the same mutation to occur independently in two neighbouring cells to be 2.48×10^9 [29]. Considering the 3D basalis glandular architecture, we speculate that upward perpendicular growth of progeny of two adjacent stem cells situated in the parallel/ branching basalis glands contribute to the regeneration of these partially mutated glands (Figure 2B). Therefore, these data conclusively confirm the existence of an endometrial epithelial stem cell (long-lived and generating clonal expansion), whereas the existence of partially mutated glands suggests that at least some endometrial glands are regenerated by more than one epithelial stem cell.

Natural history of CCO-deficient clonal unit dynamics across the ages

Age-related evolution of CCO-deficient patch formation was examined by screening 75 formalin-fixed and paraffin-embedded (FFPE) endometrial samples from women aged 21–78 years using CCO immunohistochemistry (IHC). All glands in each endometrial section were evaluated and CCO-deficient patches (defined as any CCO-deficient gland, partial, or complete) were identified in 58 of the samples (77.3%) (Figure 3A). The earliest

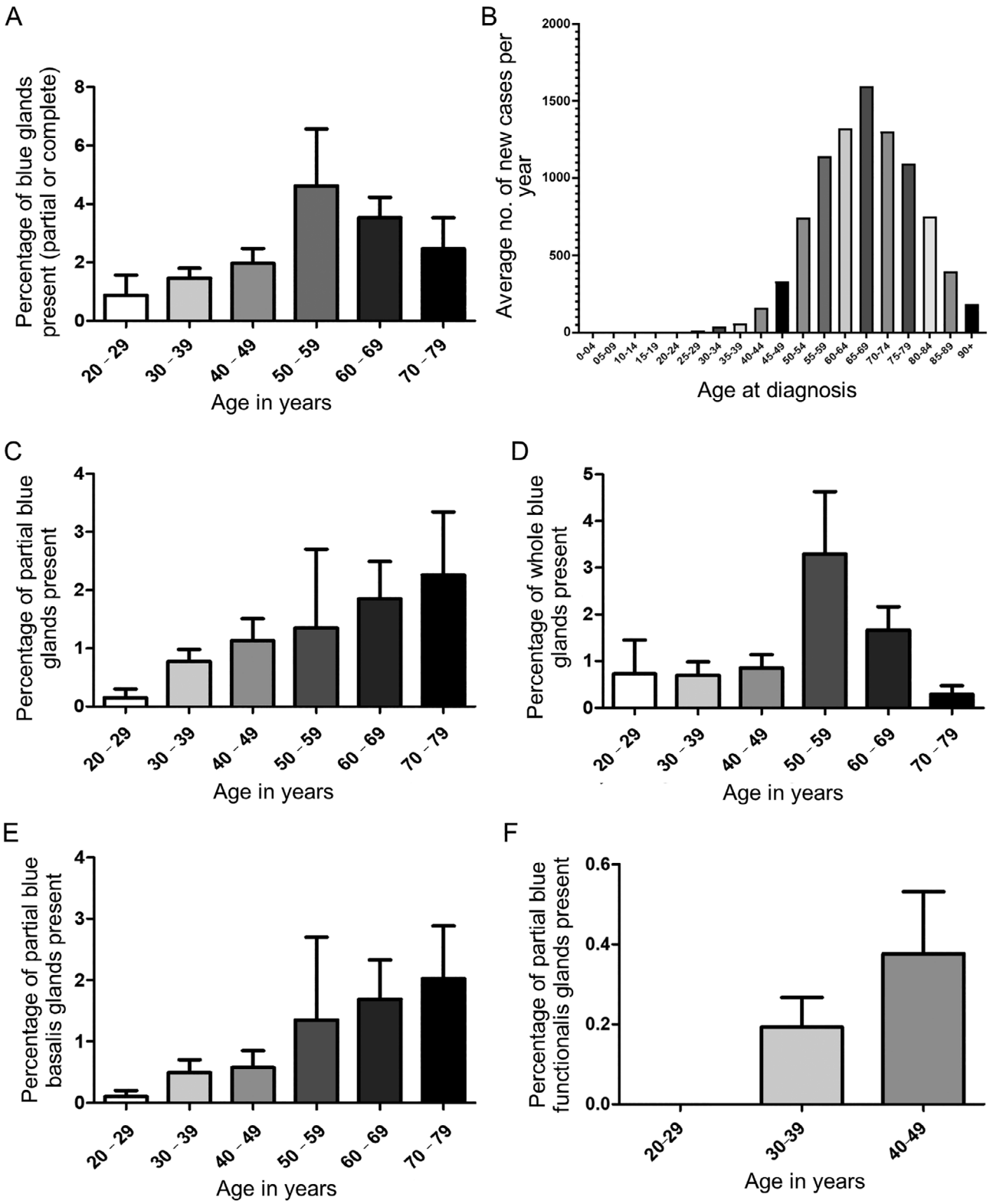

Figure 3. The proportion of pre-menopausal CCO-deficient glands increases with age. (A) The proportion of partial (heterogeneous) or complete (homogeneous) CCO-deficient clonal patches in the pre-menopausal human endometrium increases up until the age of menopause (n = 78). (B) Adapted from Cancer Research UK [30], average number of new cases of endometrial cancer per year in the UK from 2013–2015. Cases of endometrial cancer rise steeply from around age 45–49 before dropping in the oldest age groups. (C) The presence of partial CCO-deficient clonal patches (heterogeneous) in all layers of the endometrium increases with age (n = 78). (D) The presence of whole CCO-deficient clonal patches (homogeneous) in all layers of the endometrium, also increases up until the age of menopause (n = 78). (E) In the basalis layer, the presence of partial (heterogeneous) CCO-deficient clonal patches initially appear in a 25-year-old and increases with age (n = 78). (F) In the functionalis (which exists only during pre-menopausal period), partial CCO-deficient glands first appear in a 31-year-old and their percentage increases with age (n = 52).

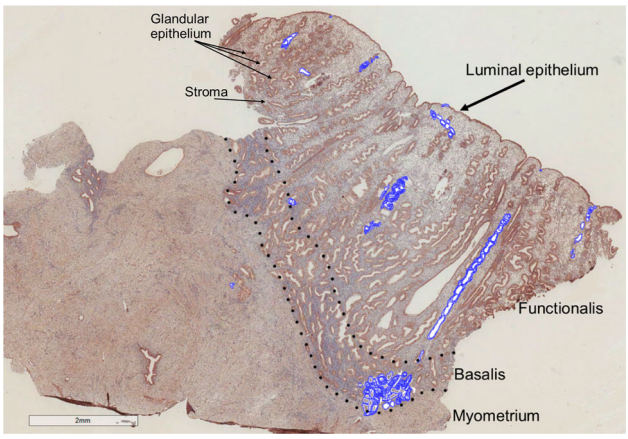

Figure 4. The extent of the CCO-deficient clonal patches suggests the basalis glands to be the location of the human endometrial epithelial stem cell niche. CCO-deficient clonal expansion across the full-thickness human endometrium was highlighted by encircling the CCO-deficient cells identified in all of the 100 consecutive sections and superimposing that image on a representative 2D image of the CCO IHC staining.

appearance of a CCO-deficient clonal patch was observed in the basalis glands of a 25-year-old (the first CCO-deficient patches in the functionalis glands appeared later, in a 31-year-old, Figure 3F), supporting the hypothesis that long-lived epithelial stem cells are located in the basalis.

Analysis of age-related evolution of CCO-deficient patches is informative with regard to dynamic parameters of stem cell turnover in the endometrium. The number of CCO-deficient clonal patches present in the functionalis and basalis of the endometrial samples increased up to menopausal age, depicting the increased endometrial stem cell turnover during the premenopausal period. Subsequent decline of CCO-deficient patches with further aging (Figure 3A,D) is explained by the induction of endometrial stem cell quiescence at menopause, where cessation of endometrial glandular proliferation and menstrual shedding occurs concluding regular regeneration. This pattern also mimics the endometrial cancer incidence curve demonstrating a 10-year time lag from the highest incidence of stem cell activity

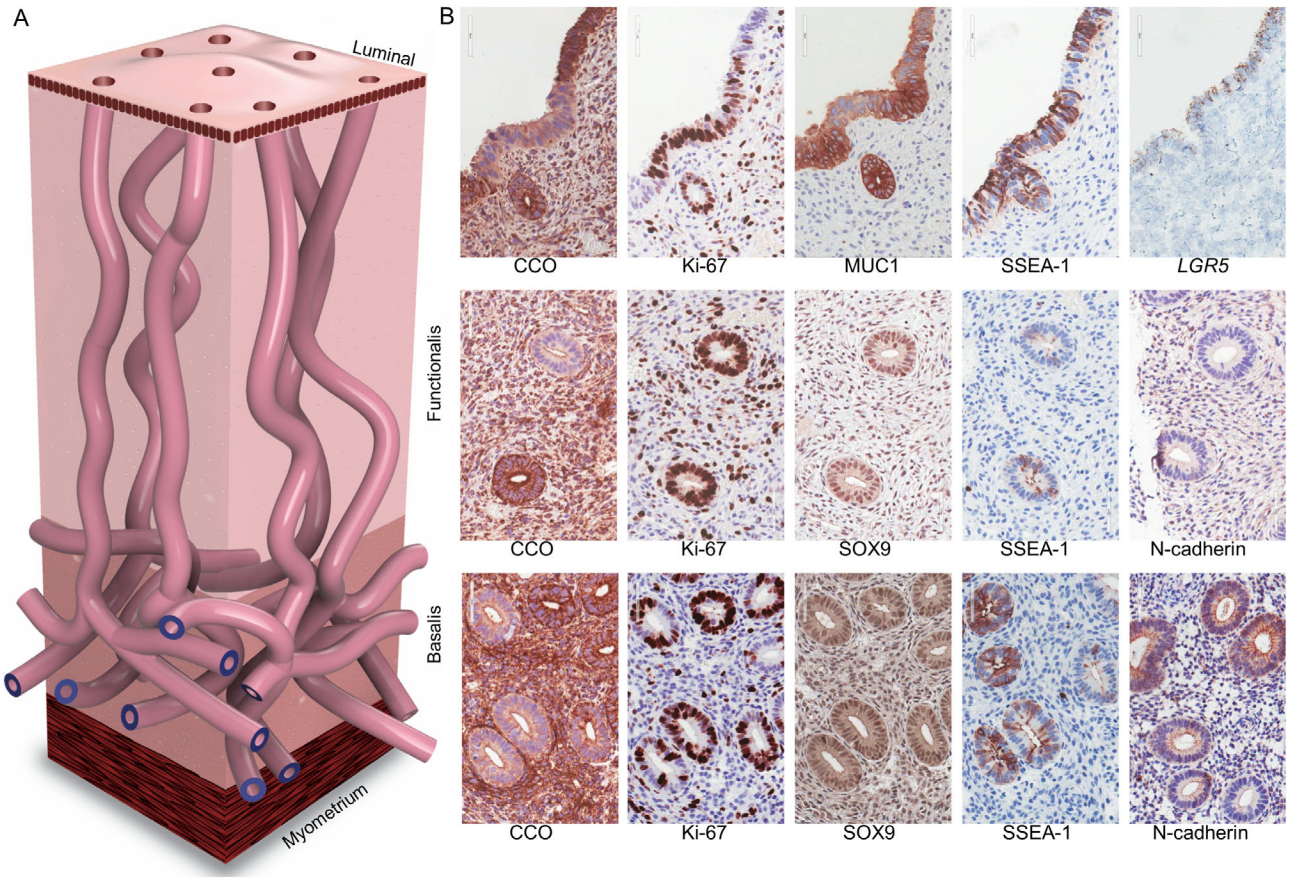

Figure 5. Proposed new schematics of multipotent stem cell-containing endometrial glands. (A) New 3D schematic demonstrates the complex basalis glands that form a branching configuration, proceeding along a horizontal course to the myometrium. (B) Representative micrographs of consecutive sections of full-thickness endometrium to demonstrate the multi-potency of endometrial epithelial stem cells; CCO-deficient epithelial cell clone contains markers in all three endometrial regions (bottom row = basalis, middle row = functionalis, and top row = luminal epithelium). CCO-deficient epithelial cells (blue cells lacking brown staining) demonstrating markers of LE (positive for MUC-1 and SSEA-1 by IHC and *LGR5* mRNA by ISH); functionalis epithelium (negative for SOX9, SSEA1, and N-cadherin by IHC) and basalis epithelium (Positive for SOX9, SSEA-1, and N-cadherin by IHC). All images 400× and scale bars = 10 μm. Supplementary material, Figure S5 shows additional representative images of whole endometrial block sections stained with the different regional markers allowing the appreciation of staining across the sample.

(reflected by CCO-deficient patch incidence) to peak incidence of endometrial cancer (Figure 3B).

Endometrial epithelial stem cells can generate all layers of the endometrial epithelium and are likely to be multipotent

The 3D models of CCO-labelled glands clearly demonstrate CCO-deficient patches residing in the basalis glands, which communicate with the functionalis CCO-deficient epithelial areas in premenopausal secretory phase endometrial samples (Figure 4 and see supplementary material, Figure S3). Because the functionalis/luminal layers are lost with menstrual shedding, the clonal patch is assumed to have arisen from the stem cells located in the basalis glands, and the stem cell producing the cells in this patch appears to have been able to generate functionalis glands in the endometrium. To confirm that all epithelial cell subtypes are encompassed by the CCO-deficient epithelial cell progeny, we demonstrated the co-expression of markers specific for the three different anatomical regions (luminal, functionalis, and basalis epithelial cells), and the regional differences in proliferative activity in the epithelium (Ki67) in CCO-deficient cells. Clonal patches of CCO-deficient epithelial cells contained markers specific to all three endometrial regions demonstrating SSEA-1, *LGR5* [22], and MUC1 [31–33] denoting LE; SSEA-1, SOX9 [1], and N-cadherin [2] marking the progenitors of the basalis glands; and absence of SSEA-1, N-cadherin, SOX9, demarcating the secretory functionalis glands [4] (Figure 5B and see supplementary material, Figure S4). We and others have shown previously that the basalis glandular cells containing SSEA-1 and N-cadherin demonstrate the ability to generate endometrial glands *in vitro*, thus they may represent the stem/progenitor population [1,2]. Furthermore, the clonal patch contained both proliferative and non-proliferative cells. These data, collectively, support that different cell subtypes comprising all human endometrial glandular regions are included in these CCO-deficient epithelial clonal patches and may have a common ancestral origin. We believe this observation suggest the existence of a multipotent endometrial epithelial stem cell (Figure 5).

Discussion

Our data have revealed the previously unknown 3D architectural organisation of the epithelial compartment in full-thickness adult human endometrium, and they directly demonstrate the existence of endometrial epithelial stem cells *in vivo*. Human endometrial glands were thought to be similar to intestinal glandular crypts; hitherto the consensus was that they assume a single, blunt ended, ductular design. We demonstrate the origin of some non-branching, single, vertical functionalis glands from a complex horizontally interconnecting network of basalis glands. Our data reported here, therefore, replaces this simple schematic of the human endometrial glandular organisation.

Although endometrial stem cell biologists have considered the basalis to be the stem cell rich layer of the human endometrium [1,34,35], the unique arrangement of these glands has been overlooked. Most recent manuscripts and frequent schematics have adopted an intestinal crypt-like basalis gland configuration for the human endometrium, with blind-ending endometrial glands resting on the sub-endometrial myometrium [34]. Our 3D reconstructions of the full-thickness human endometrial glandular compartment update this existing schematic (Figure 5A) with important functional relevance. The huge regenerative ability of the human endometrium [36] either after monthly shedding or following parturition or iatrogenic destruction (surgical ablation and curettage) is well known [37–41]. Previous scanning electron microscopy studies suggested that endometrium re-epithelialises from the remaining stumps of the basalis glands [42]. However, relying on a single blind-ending tube enriched with stem cells may not be the most efficacious arrangement, because dedicated stem cells could be easily lost/artificially removed, leading to a deficient regenerative ability in the surrounding area. Therefore, the preservation of the endometrial epithelial stem cell niche, the basalis glands, is vital. We propose that the self-preserving, self-renewing, scar-less regeneration of the human endometrium will be assisted by basalis glands assuming a complex/intricate, horizontally inter-connecting, mycelium-like network configuration. Functionalis glands, which are shed on a monthly basis, appear to sprout from the basalis glands as parallel single tubes similar to the colonic crypts [43], yet they spiral and coil, particularly during the secretory phase and thus are more complex structurally than the straight intestinal crypts. The stark differences in the 3D arrangement of non-menstruating murine endometrium [44] and the human endometrium [6,7] will allow identification of specific underlying mechanisms relevant to human embryo implantation, as well as information on the pathogenic basis for species-specific endometrial proliferative conditions, such as endometriosis. Our data therefore challenge the prevailing concept that human endometrial glands end in blind pouches in the basalis layer that contain stem cells in crypts, as in the gut mucosa. However, our histological 3D reconstruction method examines a small volume of the endometrium, within which our space-filling models demonstrate a sample of the functionalis-basalis connections. Every functionalis gland that we could trace to its destination within this volume, connected to a basalis gland. Future studies visualising larger volumes of endometrial tissue from more patients will allow us to provide further details and description of these branching basalis glands and their connections.

Our study clarifies some existing controversy on glandular clonality while providing insight into normal endometrial regeneration. Our data are of importance, since all previous studies examining glandular clonality utilised a gland extraction method that is unlikely to have

extricated the stem cell rich complex-endometrial basalis glands [3,5,45]. Our results using LCM and single cell mtDNA sequencing identified putative clonal patches spanning from the basalis to the functionalis in full-thickness endometrial samples confirming the existence of multipotent stem cells with the ability to regenerate the whole endometrial glandular element in humans. Using full-thickness human endometrium, we identified unique, sporadic, and functionally unbiased mtDNA passenger mutations elucidating monoclonal and polyclonal functionalis and basalis glands, highlighting self-propagation and renewal. We speculate that upward perpendicular growth of progeny of two adjacent stem cells situated in the parallel basalis glands is the reason for the existence of some partially mutated functionalis glands (Figure 2B). Our data therefore clarify the conflicting data on endometrial gland clonality. Furthermore, our methodology allowed examination of almost 140 000 endometrial gland profiles in a large number of endometrial samples compared with the gland extraction method in previous studies, which allowed analysis of fewer than 250 glands that exclusively included only the functionalis portions of the glands.

Recent work has depicted non-cancerous normal endometrial functionalis glands as harbouring many somatic mutations, including cancer driver mutations [45] unlike other glandular epithelium [46,47], and our data examining the natural history of non-pathological mtDNA mutations marking clonal patches corroborate their data [45,47]. The increase in number of mutated clonal patches with age up to the menopause reflects the accumulation of mutations in the stem cells and stem cell turnover/activity contributing to endometrial glandular regeneration. Because CCO mutations accumulate with age in long-lived stem cells that linger in the endometrium, the observed increase in the number of clonal patches in the premenopausal period is a surrogate marker for their contribution to the regular endometrial epithelial regeneration. The peak incidence of endometrial cancer occurring 10 years after the age where the highest proportion of CCO-deficient glands are observed (around menopause) also suggests menstruation, or shedding of the endometrial functionalis, to be a transformation protective mechanism, where progeny of the highly active stem cells with multiple mutations are effectively shed, thus preventing tumorigenesis. Stem cell activity is usually halted after menopause, but when the mutation-laden, PM stem cells are inappropriately activated with unopposed oestrogenic drive, carcinogenesis may result. Future studies should examine this possibility further.

Although the methods we employed allow for only a single snapshot in time, in a relatively small volume of a few endometrial samples, the technique does demonstrate the major aspects of stemness: multipotency and self-renewal. Because aberrations in stem cells that regularly regenerate the functionalis layer are postulated to play a role in most endometrial pathologies, expansion of our current understanding of stem cells is necessary for the development of curative treatment strategies.

Acknowledgements

This work was supported by funding from the Wellbeing of Women project grant (RTF510 NT, NAW and DKH; RG2137 DKH) and Cancer Research UK (A14895, A-MB and NAW). The authors are grateful to Jo Drury (assistance with tissue sectioning), Professor Sarah Coupland (Assistance with LCM), and John Woodward (preparing Figure 2B) of the University of Liverpool.

Author contributions statement

DKH conceived the study. NT, DKH, and NAW secured funding. NT, DKH, NAW, and MJ designed, and NT, A-MB, and CH performed, experiments. MH, DT, and DM assisted with the aligning of the 3D models. All authors interpreted data. NT and DKH wrote the first draft of the manuscript. All authors revised the manuscript critically for important intellectual content and approved the submitted final version.

References

1. Valentijn AJ, Palial K, Al-Lamee H, *et al*. SSEA-1 isolates human endometrial basal glandular epithelial cells: phenotypic and functional characterization and implications in the pathogenesis of endometriosis. *Hum Reprod* 2013; **28:** 2695–2708.
2. Nguyen HPT, Xiao L, Deane JA, *et al*. N-cadherin identifies human endometrial epithelial progenitor cells by in vitro stem cell assays. *Hum Reprod* 2017; **32:** 2254–2268.
3. Kim JY, Tavare S, Shibata D. Counting human somatic cell replications: methylation mirrors endometrial stem cell divisions. *Proc Natl Acad Sci U S A* 2005; **102:** 17739–17744.
4. Tempest N, Maclean A, Hapangama DK. Endometrial stem cell markers: current concepts and unresolved questions. *Int J Mol Sci* 2018; **19**.
5. Tanaka M, Kyo S, Kanaya T, *et al*. Evidence of the monoclonal composition of human endometrial epithelial glands and mosaic pattern of clonal distribution in luminal epithelium. *Am J Pathol* 2003; **163:** 295–301.
6. Arora R, Fries A, Oelerich K, *et al*. Insights from imaging the implanting embryo and the uterine environment in three dimensions. *Development* 2016; **143:** 4749–4754.
7. Vue Z, Gonzalez G, Stewart CA, *et al*. Volumetric imaging of the developing prepubertal mouse uterine epithelium using light sheet microscopy. *Mol Reprod Dev* 2018; **85:** 397–405.
8. Cervello I, Gil-Sanchis C, Mas A, *et al*. Human endometrial side population cells exhibit genotypic, phenotypic and functional features of somatic stem cells. *PLoS One* 2010; **5:** e10964.
9. Cervello I, Mas A, Gil-Sanchis C, *et al*. Reconstruction of endometrium from human endometrial side population cell lines. *PLoS One* 2011; **6:** e21221.
10. Chan RW, Gargett CE. Identification of label-retaining cells in mouse endometrium. *Stem Cells* 2006; **24:** 1529–1538.
11. Cervello I, Martinez-Conejero JA, Horcajadas JA, *et al*. Identification, characterization and co-localization of label-retaining cell population in mouse endometrium with typical undifferentiated markers. *Hum Reprod* 2007; **22:** 45–51.

12. Wang Y, Sacchetti A, van Dijk MR, *et al*. Identification of quiescent, stem-like cells in the distal female reproductive tract. *PLoS One* 2012; **7:** e40691.
13. Taylor RW, Barron MJ, Borthwick GM, *et al*. Mitochondrial DNA mutations in human colonic crypt stem cells. *J Clin Invest* 2003; **112:** 1351–1360.
14. Wright NA. Stem cell identification–*in vivo* lineage analysis versus *in vitro* isolation and clonal expansion. *J Pathol* 2012; **227:** 255–266.
15. Gaisa NT, Graham TA, McDonald SA, *et al*. The human urothelium consists of multiple clonal units, each maintained by a stem cell. *J Pathol* 2011; **225:** 163–171.
16. Gaisa NT, Graham TA, McDonald SA, *et al*. Clonal architecture of human prostatic epithelium in benign and malignant conditions. *J Pathol* 2011; **225:** 172–180.
17. Fellous TG, McDonald SA, Burkert J, *et al*. A methodological approach to tracing cell lineage in human epithelial tissues. *Stem Cells* 2009; **27:** 1410–1420.
18. Blackwood JK, Williamson SC, Greaves LC, *et al*. In situ lineage tracking of human prostatic epithelial stem cell fate reveals a common clonal origin for basal and luminal cells. *J Pathol* 2011; **225:** 181–188.
19. Noyes RW, Hertig AT, Rock J. Dating the endometrial biopsy. *Am J Obstet Gynecol* 1975; **122:** 262–263.
20. Dallenbach-Hellweg G. The Normal Histology of the endometrium. *In: Histopathology of the endometrium*. Springer: Berlin, Heidelberg, 1987; 25–92.
21. Kamal AM, Bulmer JN, DeCruze SB, *et al*. Androgen receptors are acquired by healthy postmenopausal endometrial epithelium and their subsequent loss in endometrial cancer is associated with poor survival. *Br J Cancer* 2016; **114:** 688–696.
22. Tempest N, Baker AM, Wright NA, *et al*. Does human endometrial LGR5 gene expression suggest the existence of another hormonally regulated epithelial stem cell niche? *Hum Reprod* 2018; **33:** 1052–1062.
23. Baker AM, Graham TA, Elia G, *et al*. Characterization of LGR5 stem cells in colorectal adenomas and carcinomas. *Sci Rep* 2015; **5:** 8654.
24. Andrey P, Maurin Y. Free-D: an integrated environment for three-dimensional reconstruction from serial sections. *J Neurosci Methods* 2005; **145:** 233–244.
25. Andrews RM, Kubacka I, Chinnery PF, *et al*. Reanalysis and revision of the Cambridge reference sequence for human mitochondrial DNA. *Nat Genet* 1999; **23:** 147.
26. Baker AM, Gabbutt C, Williams MJ, *et al*. Crypt fusion as a homeostatic mechanism in the human colon. *Gut* 2019.
27. Roberts N, Magee D, Song Y, *et al*. Toward routine use of 3D histopathology as a research tool. *Am J Pathol* 2012; **180:** 1835–1842.
28. Hempstock J, Cindrova-Davies T, Jauniaux E, *et al*. Endometrial glands as a source of nutrients, growth factors and cytokines during the first trimester of human pregnancy: a morphological and immunohistochemical study. *Reprod Biol Endocrinol* 2004; **2:** 58.
29. Lin WR, Lim SN, McDonald SA, *et al*. The histogenesis of regenerative nodules in human liver cirrhosis. *Hepatology* 2010; **51:** 1017–1026.
30. Uterine Cancer, Average number of New Cases per Year and Age-Specific Incidence Rates per 100,000 Females, UK. [Accessed 1 December 2019]. Available from: https://www.cancerresearchuk.org/health-professional/cancer-statistics/statistics-by-cancer-type/uterine-cancer/incidence#heading-One.
31. Hild-Petito S, Fazleabas AT, Julian J, *et al*. Mucin (Muc-1) expression is differentially regulated in uterine luminal and glandular epithelia of the baboon (Papio anubis). *Biol Reprod* 1996; **54:** 939–947.
32. DeLoia JA, Krasnow JS, Brekosky J, *et al*. Regional specialization of the cell membrane-associated, polymorphic mucin (MUC1) in human uterine epithelia. *Hum Reprod* 1998; **13**(1O): 2902–2909.
33. Dharmaraj N, Chapela PJ, Morgado M, *et al*. Expression of the transmembrane mucins, MUC1, MUC4 and MUC16, in normal endometrium and in endometriosis. *Hum Reprod* 2014; **29:** 1730–1738.
34. Gargett CE, Schwab KE, Deane JA. Endometrial stem/progenitor cells: the first 10 years. *Hum Reprod Update* 2016; **22:** 137–163.
35. Prianishnikov VA. A functional model of the structure of the epithelium of normal, hyperplastic and malignant human endometrium: a review. *Gynecol Oncol* 1978; **6:** 420–428.
36. Hapangama DK, Kamal AM, Bulmer JN. Estrogen receptor β: the guardian of the endometrium. *Hum Reprod Update* 2015; **21:** 174–193.
37. Gargett CE. Uterine stem cells: what is the evidence? *Hum Reprod Update* 2007; **13:** 87–101.
38. Gargett CE. Identification and characterisation of human endometrial stem/progenitor cells. *Aust N Z J Obstet Gynaecol* 2006; **46:** 250–253.
39. Tresserra F, Grases P, Ubeda A, *et al*. Morphological changes in hysterectomies after endometrial ablation. *Hum Reprod* 1999; **14:** 1473–1477.
40. Gimpelson RJ. Ten-year literature review of global endometrial ablation with the NovaSure(R) device. *Int J Womens Health* 2014; **6:** 269–280.
41. Muller I, van der Palen J, Massop-Kelmink D, *et al*. Patient satisfaction and amenorrhea rate after endometrial ablation by Thermachoice III or NovaSure: a retrospective cohort study. *Gynecol Surg* 2015; **12:** 81–87.
42. Ludwig H, Metzger H. The re-epithelization of endometrium after menstrual desquamation. *Arch Gynakol* 1976; **221:** 51–60.
43. Henrikson RC, Kay G, Mazurkiewicz JE. *The national medical series for independent study - histology*. Philadelphia, PA: Lippincott Williams and Wilkins; 1997.
44. Yuan J, Deng W, Cha J, *et al*. Tridimensional visualization reveals direct communication between the embryo and glands critical for implantation. *Nat Commun* 2018; **9:** 603.
45. Suda K, Nakaoka H, Yoshihara K, *et al*. Clonal expansion and diversification of cancer-associated mutations in endometriosis and Normal endometrium. *Cell Rep* 2018; **24:** 1777–1789.
46. Lee-Six H, Olafsson S, Ellis P, *et al*. The landscape of somatic mutation in normal colorectal epithelial cells. *Nature* 2019; **574:** 532–537.
47. Moore L, Leongamornlert D, Coorens THH, *et al*. The mutational landscape of normal human endometrial epithelium. *Nature* 2020; **580:** 640–646.

SUPPLEMENTARY MATERIAL ONLINE

Supplementary figure legends

Figure S1. Micrographs and 3D model schematics depicting 3D architecture of postmenopausal (PM) human endometrium

Figure S2. Ki67 across the menstrual cycle

Figure S3. Representative micrographs of full thickness secretory endometrium highlighting original and CCO-deficient encircled images

Figure S4. Representative micrographs of full thickness endometrium to demonstrate the multi-potency of endometrial epithelial stem cells

Figure S5. Representative images of a whole endometrial block stained for the different regional markers

Table S1. Demographic details of the patients involved in the study

Table S2. Details of antibodies used and conditions for use

Video S1. Branching horizontal basalis and non-branching vertical functionalis glands of proliferative phase endometrium. 3D reconstruction from 100 consecutive 4 μm formalin-fixed paraffin-embedded (FFPE) full thickness human endometrial tissue sections

Video S2. Branching horizontal basalis and non-branching vertical functionalis glands of secretory phase endometrium. 3D reconstruction from 100 consecutive 4 μm FFPE full-thickness human endometrial tissue sections

Video S3. Branching horizontal basalis glands of PM endometrium. 3D reconstruction from 100 consecutive 4 μm FFPE full-thickness human endometrial tissue sections

Video S4. Non-branching vertical functionalis glands of proliferative phase endometrium. 3D reconstruction from 100 consecutive 4 μm FFPE full-thickness human endometrial tissue sections

Video S5. Non-branching vertical functionalis glands of secretory phase endometrium. 3D reconstruction from 100 consecutive 4 μm FFPE full-thickness human endometrial tissue sections